Biomass Conversion and Biorefinery (2023) 13:12235–12248
https://doi.org/10.1007/s13399-021-02059-8

ORIGINAL ARTICLE

Development of ecofriendly high performance anti-corrosive chitosan nanocomposite material for mild steel corrosion in acid medium

Mohamed Hasanin[1] · **Sherief A. Al Kiey**[2]

Received: 28 July 2021 / Revised: 7 October 2021 / Accepted: 23 October 2021 / Published online: 31 October 2021

Abstract

The present study discusses preparation, characterisation and corrosion inhibition of mild steel exposed to acidic medium (1M HCl using) nanocomposite based chitosan (CH) doped with zinc oxide nanoparticles ZnO NPs. Preparation of CH-ZnONPs was carried out via facile, in situ reduction, coast effective and green method. The characterisations of the synthesised inhibitor CH-ZnONPs were evaluated using FTIR, XRD, SEM-EDX, TEM, TGA, DLS and N_2 adsorption-desorption as well as the antimicrobial activity. Results showed that CH-ZnONPs was prepared in nanoscale (26–136 nm) with surface area more than neat CH by about ten folding. Moreover, The DLS measurement results were configured high stability of the CH-ZnONPs. CH-ZnONPs was assessed as a potential corrosion inhibitor for mild steel in acid solutions 1M HCl. Experimental evaluations were carried out at various concentrations to investigate the inhibition efficiency and adsorption behaviour of CH-ZnO NPs. Electrochemical and surface investigations were used to investigate the efficiency of in inhibiting corrosion (SEM-EDX and surface roughness). The results indicated that increasing the concentration of the green corrosion inhibitor CH-ZnO NPs increased the efficiency of the used inhibitor, which reached 93.95% in the presence of 100 ppm. Furthermore, the CH-ZnO NPs functioned as a mixed-type corrosion inhibitor, according to Tafel extrapolated polarisation measurements. The Nyquist plot of impedance is mostly represented by a depressed capacitive loop with various concentrations of inhibitor. The CH-ZnONPs inhibit metallic corrosion by means of an adsorption mechanism adopting the isothermal model of Langmuir adsorption. Surface morphology examinations, in addition to electrochemical tests, result in a significant evidence for the existence of an inhibitor molecules adsorbed across the mild steel surface.

Keywords Chitosan · Zinc oxide nanoparticle · Nanocomposite · Mild steel · Corrosion inhibitor

1 Introduction

Due to their high mechanical power, tremendous availability and low cost, metals and alloys are widely used as construction supplies in many industries [1–4]. However, most metallic materials, particularly during acid cleaning and pickling processes, are extremely unstable and susceptible to corrosive degradation when exposed to aggressive electrolytes [5–7]. Corrosion is a serious issue in the oil and gas sector, as it accounts for a large amount of the company's total costs each year. It causes leaks in pipelines, tubing, tanks and other equipment, causing in process shutdowns, contamination and significant financial losses. The rock reservoir stimulation technique is used to boost productivity utilising hydrochloric acid, formic acid, hydrofluoric acid and acetic acid in the gas and oil drilling industry's most significant stage, well acidizing. In particular, HCl solutions are widely employed for scale removal treatments to remove carbonated minerals and iron oxides [8]. HCl is frequently employed for acidifying treatments due to the formation of metal chlorides, which are extremely soluble in the aqueous media [9–11]. Other acids are less effective than HCl because phosphate, nitrate and sulphate salts are less soluble in aqueous solutions than chloride salts [12]. As a result, equipment must be protected at all times when operating with acidic fluids. Corrosion scientists and engineers are currently developing and implementing many methods of corrosion

Mohamed S. Hasanin and Sherief A. Al Kiey equally contributed.

✉ Sherief A. Al Kiey
sheriefalkiey@yahoo.com

[1] Cellulose and paper Department, National Research Centre, Dokki, Cairo 12622, Egypt

[2] Electrochemistry and corrosion Laboratory, National Research Centre, Dokki, Cairo 12622, Egypt

safety to protect metal deterioration such as coating, alloying, inhibitors and dealloying [13–16]. The application of organic compound as corrosion inhibitors is one of the most prominent, efficient and economical possible methods due to their simple and cost-effective synthesis, in addition to their high inhibition efficiency and ease of application [17–25]. Most of the organic inhibitors, however, are poisonous in nature and their synthesis involves multi-step. Plant extracts, amino acids, carbohydrates and their derivatives may also be used as alternate sources of conventional corrosion inhibitors that are environmentally friendly. Multiple carbohydrates and their derivatives have recently been identified as effective metal and alloy corrosion inhibitors [26–29]. The existence of polar functional groups increases their effectiveness in corrosion inhibition by increasing their molecular size and increasing their solubility in polar electrolytes. Looking forward, the environmentally friendly behaviour, synthesis, characterisation and utterance of carbohydrates and their derivatives in polar electrolytic media, including HCl and H_2SO_4, polar functional groups may also promote the solubility of carbohydrate polymers. Biopolymers are the largest category of carbohydrates, which produced or extracted from living organisms [30, 31]. Chitosan is the one of promising biopolymers with unique by the amino group active towered, reaction, modifications, biological activity and fitted with various applications [32, 33]. Due to their natural and biological origin, chitosan and its derivatives, similar to carbohydrates, can be considered bio-inspired and bio-degradable materials suitable for various industrial applications, including corrosion inhibition [34, 35]. Nanomaterials doped biopolymer is the new trend of science which produced the new materials characterised by both features of neat source as well as overcome the drawbacks of the native materials [36–38]. In a variety of applications, zinc oxide nanoparticles (ZnO NPs) have been proposed as an effective antibacterial agent. Their biological toxicity and environmental effects, on the other hand, have restricted their practical application [39, 40]. To address this, NPs are combined with antimicrobial polymers to minimise cytotoxicity while also improving stability and performance without compromising their functional properties. Chitosan contains a lot of hydroxyl and amino groups, so it is a decent potential inhibitor, but little is known about how it works [41].

Herein, environmentally benign CH-ZnO nanocomposite was synthesised by green, facile method and tests its corrosion inhibition effect on mild steel corrosion in acidic medium 1M HCl. The effectiveness of corrosion inhibition of CH-ZnONPs composite was demonstrated using experimentation. The novelty of this study lies in the fact that the synthesised CH-ZnONPs composite acted as an efficient corrosion inhibitor with an inhibition efficiency of 93.95% at a concentration of as low as 100 ppm. Moreover, the antimicrobial activity was investigated and observed the high antimicrobial effect against the most population of microorganisms. Chitosan and its derivatives can be considered one of the green ones because of their biodegradability, biocompatibility, enormous abundance, natural and biological origin and high solubility in polar media.

2 Methodology

2.1 Materials

Medium molecular weight chitosan (degree of deacetylation, 75–85%), and zinc acetate were obtained from Sigma-Aldrich. All chemicals and media as well as reagents were purchased from Sigma-Aldrich in analytical grade.

2.2 Methods

2.2.1 Preparation of CH-ZnONPs

One mole of zinc acetate was dissolved in 0.1N acetic acid solution. Chitosan (0.1 g) was dissolved in the previously prepared solution and continuous steering at 1500 rpm for 3h at room temperature. The collected solution was irradiated by microwaves (1kW) for 3 min, then sonicated for 45 min in a sonicated water bath at 60°C. The solution was lyophilized and maintained in the refrigerator for further investigations.

2.2.2 Characterisations of prepared CH-ZnONPs

FTIR spectra were recorded in the frequency range 400–4000 cm^{-1} with a resolution of 4 cm^{-1} using FTIR 6100 Jasco Japan Spectrum equipment. The XRD patterns of chitosan, and the prepared composite were investigated on a Diano X-ray diffractometer using CuK_{α} radiation source energised at 45 kV and a Philips X-ray diffractometer (PW 1930 generator, PW 1820 goniometer) with CuK radiation source (λ =0.15418 nm). The surface morphology, as well as elemental distribution of prepared composite, was studied using the non-destructive energy dispersive X-ray (EDX) unit attached to scanning electron microscopy (Quanta FESEM 250). For surface morphology, imaging of different samples was recorded using an accelerating voltage of 10–15 kV. The microstructures were observed by transmission electron microscope (TEM, JEOl JEM2100). TGA was carried out using the TGA Q500 device. NICOMP 380 ZLS, Dynamic light scattering (DLS) instrument (PSS, Santa Barbara, CA, USA), using the 632 nm line of a HeNe laser as the incident light with angle 90° and zeta potential with external angle 18.9°. Nitrogen adsorption–desorption measurements were carried out at 77.35 K on a Nova Touch LX4Quantachrome, USA, to determine the Brunauer–Emmett–Teller (BET) and

Barrett, Joyner, Halenda (BJH) surface area. Before measurement, the samples were kept in a desiccator until testing. Samples were cooled with liquid nitrogen and analysed by measuring the volume of gas (N_2) adsorbed at specific pressures. The pore volume was taken from the adsorption branch of the isotherm at $P/P_O = 0.995$ assuming complete pore saturation.

2.2.3 Electrochemical measurements

The inhibitory role of CH-ZnONPs composite on mild steel corrosion in 1 M HCl was studied using electrochemical methods. The electrochemical studies were carried out using three-electrode system in which, platinum acts as a counter, Ag/AgCl (Sat. KCl) acts as a reference electrode, and mild steel specimens were used as working electrodes. The working electrodes were permitted to corrode freely in the absence and presence of CH-ZnONPs composite for 60 min prior to the start of electrochemical measurements. The electrochemical impedance spectroscopy (EIS) studies were carried out at OCP in the frequency range from 100 KHz to 10 mHz.

In order to acquire polarisation resistance (Rp) values by which the inhibition efficiency of CH-ZnONPs composite was evaluated using the following relationship, the EIS data were fitted into an effective equivalent circuit as shown in equation (1) [22, 25]:

$$IE(\%) = \frac{Rp(inh) - Rp}{Rp(inh)} \text{ x } 100 \quad (1)$$

Potentiodynamic polarisation studies on mild steel corrosion in 1 M HCl with and without CH-ZnONPs composite was performed by recording anodic and cathodic Tafel curves (at a scan rate of 1 mV/s). In order to obtain the values of corrosion current density *i* from which percentage inhibition efficiency is achieved, linear segments of anodic and cathodic Tafel curves were extrapolated as shown in Equation (2) [22]:

$$\eta_{Tafel}, \% = \left(i - \frac{i}{i_o}\right) \times 100 \quad (2)$$

2.2.4 Surface morphology

SEM and roughness measurements were considered for the analysis of the microstructure of the mild steel material. After 48 h of dipping, the mild steel samples were taken and then distilled water washed and dried for the coupons. The Quanta FEG 250 and Gwyddion 2.45 software scoping for SEM and the roughness of the inhibitor were subsequently tracked for the test micrographs.

2.2.5 Antimicrobial evaluation

Cultures of the following microorganisms were used in the tests: (i) Gram-negative bacteria: *Escherichia coli* (*NCTC-10416*); (ii) Gram-positive bacteria: *Bacillus subtilis* (*NCID-3610*); (iii) unicellular fungi: namely, *Candida albicans* (NCCLS 11) using the nutrient broth medium; (vi) filamentous fungi: namely, *Aspergillus Niger* (ATCC-22342). The antimicrobial studies were carried out via colony formation unite (CFU) method according to our previous finger [42, 43] to judge the antimicrobial activity.

3 Results and discussion

3.1 Physicochemical characterisations of CH-ZnO NPs

3.1.1 Fourier transform infrared spectroscopy analysis

The characterisation of prepared CH-ZnONPs nanocomposite, as well as native chitosan, includes FT-IR, XRD, SEM, TEM, TGA and DLS. The FT-IR spectra were illustrated in Figure 1A. FT-IR spectrum of chitosan was observed the characteristic bands at 3431, 2941, 1649, 1516 and 1016 cm^{-1} attributed to N–H and OH symmetric stretching, vibration as well as inter- and intra-molecular hydrogen bonds, C–H starching, carbonyl (C=O–NHR) and an amine group ($–NH_2$) and saccharide structure band, respectively [31, 33]. In addition, the incorporation of ZnO NPs in the chitosan structure is affecting the FT-IR spectrum significantly. The OH band was shifted to lower frequency; a 3111 cm^{-1}, as well as the bands at 1649 and 1516 cm^{-1}, was overlapped to appear in CH-ZnONPs at 11556 cm^{-1}. These changes are due to effects of interaction of ZnONPs with an active group of chitosan chains. On the other hand, the band-characterised ZnO was observed as new bands in CH-ZnONPs at 885, 662 and 450 cm^{-1} corresponding for weak vibration of Zn–O [44], secondary Zn–O bond vibration and ZnO symmetric bending vibration. These previous investigations were conformed the repression of CH-ZnONPs.

3.1.2 X-ray diffraction spectrometry

Crystallographic study of the neat chitosan, as well as nanocomposite, was carried out to investigate the crystallinity as well as the interaction between biopolymer and metal oxide. Figure 1B observes the XRD patterns of testing samples. Chitosan pattern was illustrated as typical chitosan as remarked in other literatures with two hump peaks at around 2θ values of 11.0° and 20.2°. In contrast, the CH-ZnONPs pattern was emphasised the present of ZnO nanoparticles. The peaks of 2θ from 30° to 40° assigned to the (1 0 0), (0

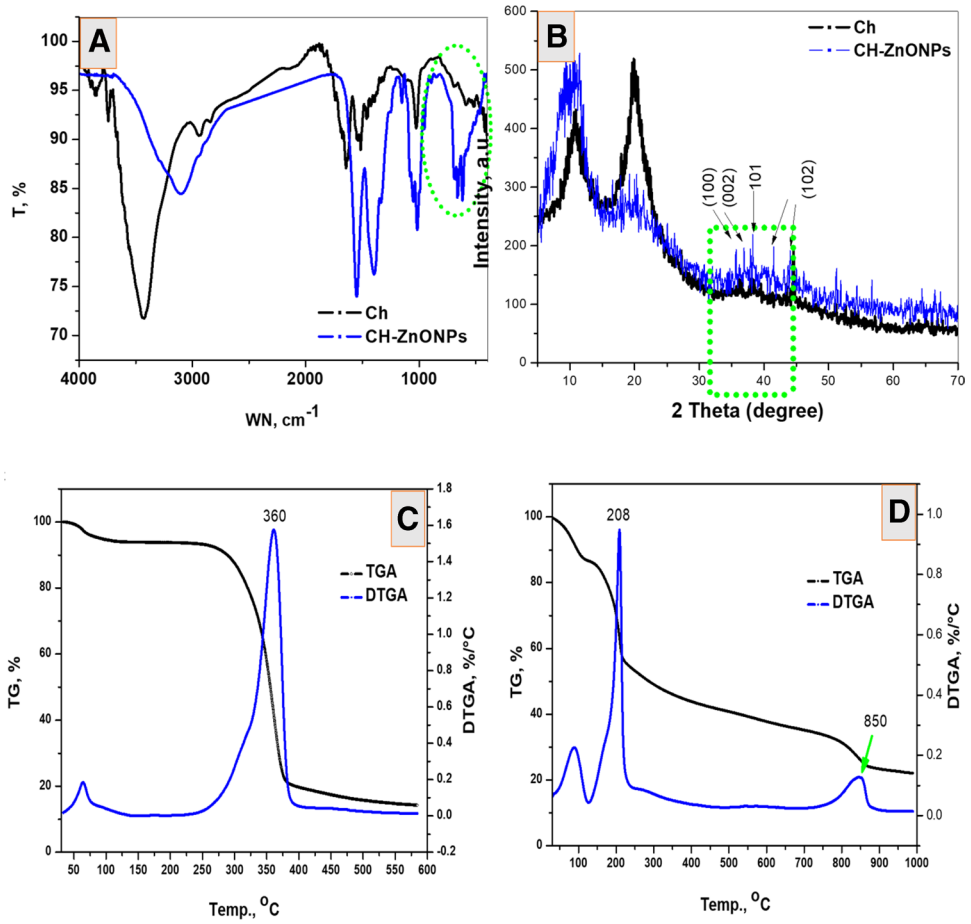

Figure 1 **A** FT-IR of neat chitosan and CH-ZnONPs. **B** XRD of neat chitosan and CH-ZnONPs. Thermal analysis of neat chitosan (**C**) and CH-ZnONPs (**D**).

0 2) and (1 0 1). Moreover, the weak peaks at 56.59°, 62.7° and 67.90° were assigned to the (1 0 0), (0 0 2) and (1 0 1), respectively. This crystallography was in agreement with those of the hexagonal wurtzite structure of ZnO (JCPDS card 36-1451).

3.1.3 Thermogravimetric analysis

The thermal study includes the TGA and DTGA of the neat chitosan as well as nanocomposite. Figure 1(C, D) illustrates the thermal behaviours of testing samples. Figure 1C observes one stage of chitosan decomposition with peak at 360°C as well as the start and end were 235 and 400°C, respectively. However, the remaining weights for each point were recorded 58, 53 and 18.3%, respectively. This thermography was typical biopolymer behaviour. On the other hand, the nanocomposite was observed two stages of decomposition (Figure 1D). Stage one was started at 130°C and end at 242°C with peak at 208°C. The second stage was started at 755°C and end at 892°C which peak recorded at 850°C. The remaining weights for peaks of two stages were 58 and 26%, respectively, with high remaining weight percentage in comparison with neat chitosan as a result to ZnO. Moreover, the presence of ZnONPs is affecting the decomposition stage where the decomposition of chitosan was enhanced by addition of ZnONPs as well as the highest remaining weight percentage. In this context, the final remaining weight percentage in nanocomposite was elevated to 23% in comparison with the other in neat chitosan (12%).

3.1.4 Topography study of CH-ZnONPs

The topography study was included SEM, EDX, mapping and TEM. SEM image was clarified the surface structure of nanocomposite (Figure 2A) which performed as rough surface with uniformed texture with spots have metallic chain like in nanoscale is ZnONPs. EXD and mapping (Figure 2B) were observed the molecular structure as well as distribution of Zn metal over the composite surface which confirmed that the presence of C, O, N and Zn with a homogeneous distribution onto the nanocomposite surface. Additionally, TEM image (Figure 2C) was emphasised the nanostructure of the prepared composite with range 136–26nm. Moreover, the diffraction pattern (Figure 2D) was affirmed the crystallinity referred to metal oxide presences.

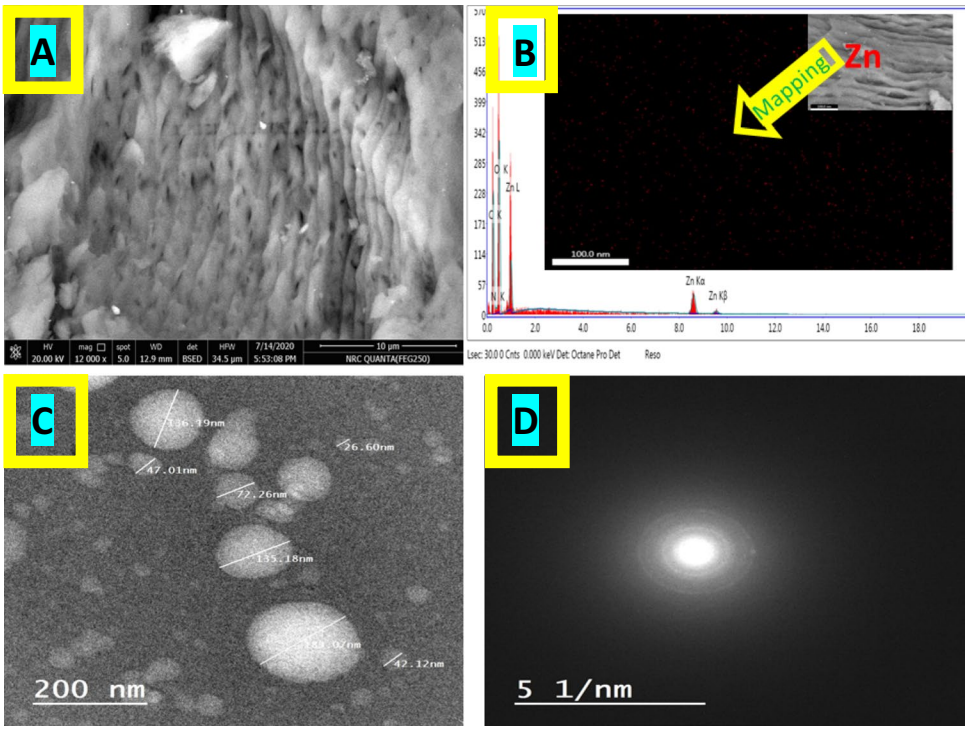

Figure 2 Topographical study of nanocomposite. SEM (**A**), EDX and mapping (**B**), TEM (**C**) and diffraction of the nanocomposite (**D**).

Table 1 DLS measurements of neat chitosan and CH-ZnONPs.

Sample	Average zeta potential, mV	Average particle size, nm	PDI
Ch	9	833	0.49
CH-ZnONPs	31	136	0.23

3.1.5 DLS measurements

Dynamic lights scattering measurements were evaluated to demonstrate to evaluate the particle behaviours and stability in a colloidal solution. The obtained results were tabulated in Table 1. The neat chitosan sample was performed as typical macromolecule with average particle size in micron scale with low Polydispersity Index (PDI) value which is an indication of their quality with respect to the size distribution. In contrast, the CH-ZnONPs was performed the low average particle size about 136 nm with high stability, according to the PDI value [21, 45]. On the other hand, average zeta potential measurement was emphasised the particle size data where the neat Ch and CH-ZnONPs values were 9 and 31 mV, respectively, as refer to the high stability of the CH-ZnONPs than the neat chitosan in colloidal solutions. These results affirm the pervious conclusion from above characterisations.

Table 2 Surface area measurements of neat chitosan and CH-ZnONPs.

Sample	BET, m^2/g	Average pore diameter, nm	BJH, cm^2/g	Pore volume, cm^3/g	Total pore volume, cm^3/g
Ch	2.2	95.3	7.11	0.023	2.059
CH-ZnONPs	209.1	15.7	25.4	0.052	160.3

3.1.6 Surface area measurements

The surface area measurements were included BET, average pore reduces, BJH, pore volume and total pore volume. Table 2 illustrates the obtained results which confirmed that the molecular structure of CH-ZnONPs is in small size in comparison with neat CH. Moreover, The BET, as well BJH surface area measuring, was observed the high surface area in mesopores as well as micropores for CH-ZnONPs. Additionally, average pore reduces of CH-ZnONPs sample is less than neat chitosan by more 6-fold. In addition, the pore volume, as well as total pore volume, was increased as results in preparation of the CH-ZnONPs. These results overall conformed the effect of addition of ZnONPs to net chitosan is affecting the converted the new production as nanocomposite with excellent surface and molecular structure.

3.2 Electrochemical measurements

3.2.1 Electrochemical impedance measurements

The corrosion mechanism was represented by electrochemical impedance spectroscopy (EIS), which provided kinetic information at the metal/solution contact. The relationship between frequency and impedance was studied in this study. EIS experiments were performed to study the corrosion behaviour of mild steel in 1 M HCl solution without or with the applied inhibitor. The impedance spectra of mild steel in the acidic solution (1M HCl) without or with different CH-ZnONPs concentrations are shown in Figure 3 at room temperature. Table 3 displays the electrochemical parameters obtained from the fitting of the EIS curves into an effective equivalent circuit Figure 3D.

From Figure 3, it can be shown that Nyquist curves (with and without CH-ZnONPs nanocomposite) reflect a single depressed semicircle, indicating that a charge transfer phenomenon is involved in mild steel corrosion with and without

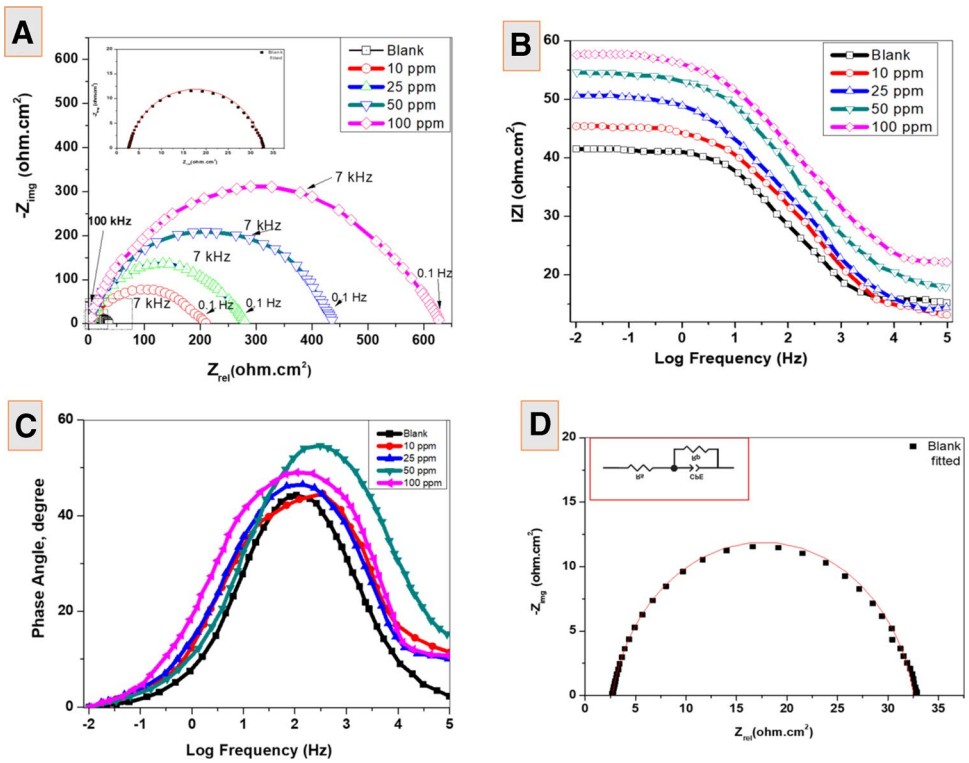

Figure 3 Nyquist (**a**) and Bode modulus and phase angle plot (**B**, **C**) of mild steel corrosion in the presence and absence of inhibitor (CH-ZnONPs) and (**D**) representative of example simulation of Nyquist blank (inset the equivalent circuit).

Table 3 Electrochemical impedance parameters for the corrosion of mild steel in the absence and presence of different concentrations of CH-ZnONPs at 25°C.

	R_s[a] (ohm.cm^2)	R_p[b] (ohm.cm^2)	C_{dl}[c] (μF/cm^2)	n[d]	CPE[e] (S.s^n/cm^2)	Goodness of fit (χ^2)	θ	I.E %
Blank	1.46	41.82	114.1	0.83	310.12	0.00413	-	-
10 ppm	1.01	241.08	93.35	0.83	205.18	0.00342	0.828	82.81
25 ppm	1.53	329.04	87.15	0.81	172.12	0.0081	0.859	85.93
50 ppm	1.39	484.2	47.21	0.87	95.17	0.0074	0.914	91.48
100 ppm	1.46	686.64	43.94	0.89	82.27	0.0032	0.939	93.95

χ^2 means the fitting error represents the deviation between experimental data and the fitted (less than 10^{-3}), indicating that the equivalent circuit model is applicable

[a]The standard deviation range for R_s values is between 1 and 8%

[b]The standard deviation range for R_{ct} values is between 3 and 8%

[c]The standard deviation range for C_{dl} values is between 1 and 9%

[d]The standard deviation range for n values is between 6 and 8%

[e]The standard deviation range for CPE values is between 43 and 7%

inhibitors. The addition of CH-ZnO NPs to the acidic environment significantly increased the width of capacitive loops, indicating that a barrier film generated by inhibitor molecules at the mild steel-solution interface improved R_p and so effectively inhibited mild corrosion. Furthermore, as the concentration of CH-ZnO NPs increases, the radius of the capacitive loops increases [46]. The adsorption of CH-ZnONPs composite molecules at the metal-electrolyte interfaces and the development of the inhibitor barrier can be due to an increase in the diameter of the Nyquist curves. This result implies that CH-ZnONPs effectively adsorb mild steel and acid solution at the interface [47, 48]. Figure 3c shows Bode plot of the electrode in the test solution without inhibitor and with different concentrations of CH-ZnO NPs present only one time constant. The increasing concentration of CH-ZnONPs results in an increase in the impedance and phase angle of the Bode modulus for the Bode plots, demonstrating the delay in the corrosion process and increasing the inhibitory power of CH-ZnO NPs for mild steel corrosion inhibition [49, 50]. The slope of the linear relationship between log |Z| and log frequency approaches 1 as the concentration of CH-ZnO NPs increases, and the phase angle approaches 90°, indicating typical capacitive behaviour. This shows that CH-ZnO NPs adsorbed on active sites on the mild surface to form a dense film to inhibit the transport of corrosive substances. Figure 3C,D shows that the phase angle and *Z* in the CH-ZnO NPs containing solutions were changed toward more negative angles and higher impedance values, respectively, compared to the blank solution. The concentration of CH-ZnO NPs had a significant impact on the phase angle and *Z* values, similar to the Nyquist plots. This pattern implies that the mild steel resistance increased proportionately with the inhibitor concentration due to increased surface covering. In reality, at greater concentrations, there are enough CH-ZnO NPs molecules to cover a large surface area of mild steel, effectively blocking most corrosion reaction sites. The typical equivalent circuit illustrated in Figure 3D was applied to fit EIS results, where R_s is the solution resistance, R_p and *CPE* are the polarisation resistance and the constant phase element representing the capacitance of the electrical double layer and adsorbed inhibitor film.

In the present study, polarisation resistance (R_p) was used instead of using charge transfer resistance (R_{ct}), as R_p provides more details than R_{ct} [51]. A better approximation is provided by the implementation of *CPE* for metallic corrosion in aqueous electrolytes. The *CPE* (Z_{CPE}) impedance can be measured as follows [52]:

$$Z_{CPE} = A^{-1}(i\omega)^{-n} \tag{3}$$

where A is the coefficient of proportionality; ω is the angular frequency; i is the imaginary number and n is an exponent of *CPE* interrelated with the surface heterogeneity of the mild steel. Phase shift (n) provides data on the morphology of the surface since its highest value is associated with the high smoothness of the surface. When $1.0 \geq n > 0.5$, *CFE* represents a Warburg impedance (W) if the n value is around 0.5; and the last case, Q can be represented as the conductance if the n value is much lower than 0.5 and higher than 0.0 and when n more than 0.5, it acts as pseudo-capacitor. It can be seen from Table 3 that the n values did not display any significant improvement. Careful evaluation of the results showed that n values are similar to unity, which means that *CPE* acts as a pseudo-capacitor in the current analysis [53].

The double-layer capacitance (C_{dl}) values were determined using the following equation [54, 55]:

$$f(-Z\max) = \frac{1}{2\pi C\mathrm{dl}\ R\mathrm{ct}} \tag{4}$$

Table 3 summarises all of the EIS parameters for the blank and CH-ZnONPs solutions. Table 3 shows that the C_{dl} values decreased while the R_p values increased in order to increase the CH-ZnONPs concentrations. Inhibitor-containing solution, R_p values are seen to be much higher than inhibitor-free solution values. For example, after adding 10 ppm CH-ZnONPs, the value increases from 41.82 to 241.08 (ohm.cm^2), and the corresponding inhibition efficiency value reaches 82.81%. The value rises to 686.64 (ohm.cm^2) by increasing the CH-ZnONPs concentration of 100 ppm, and the corresponding value reaches 93.95%, whereas C_{dl} decreased with increasing the concentration of CH-ZnONPs from 93.35 (μF/cm^2) at 10 ppm CH-ZnONPs to 43.94 (μF/cm^2) at 100 ppm CH-ZnONPs. This demonstrates that CH-ZnO NPs can adsorb firmly to the mild steel-HCl surface. Due to the adsorption and desorption of water molecules from the mild steel surface, the value of C_{dl} was also dramatically reduced in the presence of CH-ZnO NPs [56]. Because water molecules have a lower volume and higher permittivity than inhibitor molecules, the C_{dl} value of an electrode is claimed to drop in the presence of chloride containing solutions. The decrease in C_{dl} could be attributable to a decrease in the local dielectric constant and/or an increase in the thickness of the adsorbed layer due to an increase in aggressive anion concentration.

3.2.2 Potentiodynamic polarisation measurements

Potentiodynamic polarisation measurements were used to study the corrosion kinetics process of mild steel in acidic solution without or with inhibitors. Figure 4 reflects the Tafel polarisation curves for mild steel corrosion in 1 M HCl with and without inhibitor CH-ZnONPs and Table 4 presents various extracted electrochemical polarisation parameters.

Observe carefully of Figure 4 shows that in the presence of the inhibitor (CH-ZnONPs) nanocomposite, the nature of

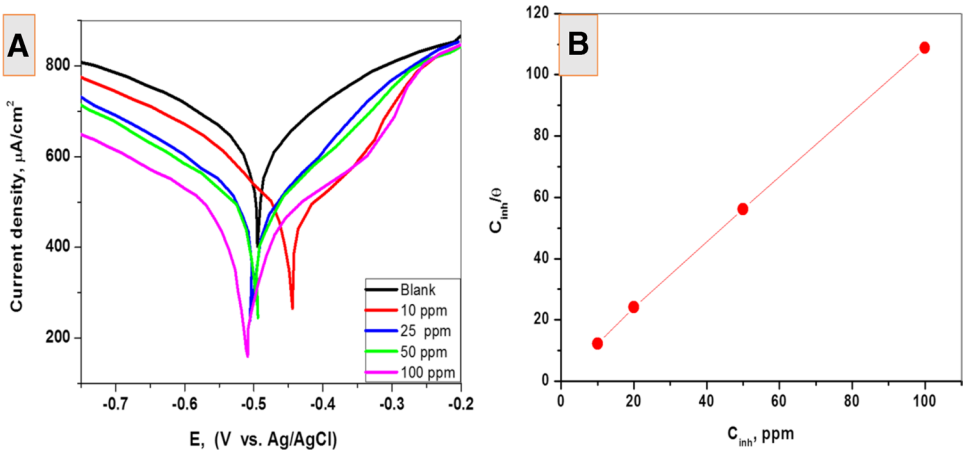

Figure 4 **A** Potentiodynamic polarisation curves of mild steel in 1 M HCl solution with different concentrations of CH-ZnONPs at 25 °C. **B** Langmuir adsorption isotherm of CH-ZnONPs composite for corrosion inhibition of mild steel in 1 M HCl.

Table 4 Polarisation parameters and the corresponding inhibition efficiencies for the corrosion of mild steel in 1 M HCl containing different concentrations of CH-ZnONPs at 25°C.

Conc.,	$-E_{corr}$ (mV)	i_{corr} (μA.cm^{-2})	β_a (mV)	$-\beta_c$ (mV)	Rp ohm.cm^2	θ	I.E.%
Blank	493.3	542.10	101.2	110.8	42.42	-	-
10 ppm	443.2	108.42	79.5	125.4	234.69	0.82	82.6
25 ppm	499.5	87.27	75.2	126.1	315.94	0.83	83.9
50 ppm	495.1	58.00	66.8	114.2	493.53	0.89	89.3
100 ppm	511.3	41.19	76.4	120.5	640.10	0.92	92.4

anodic and cathodic curves is greatly influenced, indicating that CH-ZnONPs nanocomposite exert adverse effects on both anodic and cathodic reactions. This reveals that adding the synthesised CH-ZnO NPs corrosion inhibitors to a 1M HCl solution has no effect on the reaction mechanism of mild steel. The electrochemical parameters presented in Table 4 showed a decrease in corrosion current density i_{corr} as the concentration of CH-ZnONPs increased [57, 58]. In the blank solution, for instance, the i_{corr} value is 542.1 (μA.cm^{-2}), while after adding 100 ppm CH-ZnONPs, the value is 41.19 (μA.cm^{-2}). This confirms the high performance of the natural polymers in the acid solution to protect mild steel against corrosion attack. In addition, with rising concentrations of CH-ZnONPs, the inhibition efficiency value increases considerably. This result suggests that CH-ZnONPs use their electron-rich centres to effectively adsorb and form protective films on the active sites over the metallic surface. The presence of CH-ZnONPs can be seen to have significantly affected the anodic (βa) and cathodic (βc) Tafel slope values without any substantial improvement in the corrosion potential value (E_{corr}) [57]. The values of polarisation resistance, R_p, were calculated using the following equations and the vales were recorded in Table 4 as follows:

$$R_P = \frac{1}{j_{Corr}}\left(\frac{\beta_c.\beta_a}{2.3(\beta_c+\beta_a)}\right) \quad (5)$$

From the values of R_p, as concentration of inhibitor increases, the corrosion resistance increases due to increase the surface coverage of inhibitor; hence, inhibition efficiencies increase. Depending on the displacement of the E_{corr} value of inhibited curves with respect to the uninhibited one, an inhibitor may be categorised as an anodic or cathodic form. If the displacement is more than −85 mV, the inhibitor may be categorised as an anodic or cathodic form. The displacements in E_{corr} values at all studied concentrations are less than −85 mV in the current analysis. This observation shows that both CH-ZnONPs acted as corrosion inhibitors of the mixed form.

In the presence of CH-ZnO NPs, the corrosion prevention mechanism of mild steel can be described as two half-reactions. In an acidic environment, anodic dissolution of mild steel occurs the reactions that follow:

$Fe + Cl^- \rightarrow (FeCl^-)_{ads}$

$(FeCl^-)_{ads} \rightarrow (FeCl)_{ads} + e^-$

$(FeCl^-)_{ads} = (FeCl^+) + e^-$

$(FeCl^+) \rightarrow Fe^{2+} + Cl^-$

Because of their higher electron density, the nitrogen and oxygen atoms of CH-ZnO NPs molecules can be protonated in the 1 M HCl solution. As a result, the protonated CH-ZnO NPs molecules (CH-ZnO NPs$^+$) can be easily adsorbed at the anodic site, as shown below:

$(FeCl^-)_{ads} + (CH\text{-}ZnO\ NPs^+) \rightarrow (FeCl - CH - ZnO\ NPs^+)_{ad}$

3.3 Adsorption parameters

Isothermal adsorption is an important aspect of the inhibition of metallic corrosion to explore the model of interaction between inhibitor molecules and metallic surface. In the present analysis, several widely used adsorption isotherm models, such as Langmuir, Freundlich, Frumkin and Flory-Huggins adsorption isotherms, were used to test the adsorption behaviour of the CH-ZnONPs in which Langmuir adsorption isotherm was better suited. The value of the regression coefficient (R^2) that was nearer to unity for the Langmuir adsorption isotherm model was the criterion behind the selection of the best adsorption isotherm. As follows, the Langmuir adsorption isotherm can be described as [59, 60]:

$$\frac{C_{inh}}{\theta} = \frac{1}{K_{ads}} + C_{inh} \tag{6}$$

where C_{inh} and θ are the concentration and surface coverage of CH-ZnONPs, K_{ads} is the equilibrium constant of adsorption-desorption.

For mild steel corrosion in 1 M HCl, the Langmuir adsorption isotherm plot (C_{inh}/θ vs. C_{inh}) is shown in Figure 4B. The regression coefficient values ($R^2 = 1$) were very similar to unity, validating this approach's suitability. The following equation [22, 61] was used to measure ΔG°_{ads} values using K_{ads}:

$$K_{ads} = \left(\frac{1}{55.5}\right)\exp\left(\frac{-\Delta G^{o}_{ads}}{RT}\right) \tag{7}$$

Below, the numerical value of 55.5 is the water concentration (mol /L), T is the absolute temperature and R is the constant of the universal gas. The estimated values of ΔG°_{ads} for CH-ZnONPs composite were −42.43 kJ /mol. The high negative values of ΔG°_{ads} suggest that CH-ZnONPs composite communicate effectively with the surface of the metal [62]. In addition, it can be shown that the values of ΔG°_{ads} are greater than −40 kJ/ mol, suggesting that the chemisorption system is involved in the interactions of inhibitor CH-ZnONPs composite molecules with the metallic surface [63, 64].

3.4 Effect of temperature

The effect of temperature on the corrosion process was evaluated by measuring the polarisation curve, which not only defines the adsorption efficiency of CH-ZnONPs on the mild steel surface but also shows the temperature-increasing stability of these inhibitors. Figure 5B illustrates the inhibition efficiencies of 100 ppm CH-ZnONPs at various temperatures. With the increasing concentration of CH-ZnONPs nanocomposite, it is shown that the values of inhibition efficiency decrease with the rising temperature. Using Arrhenius and transition state equations [65, 66], the effect of temperature on the inhibition effect of CH-ZnONPs nanocomposite can be described:

$$i_{corr} = A\exp\left(\frac{-Ea}{RT}\right) \tag{8}$$

where A is the frequency factor and (E_a) is the apparent activation energy.

Furthermore, it is possible to obtain activation enthalpy (ΔH_a) and activation entropy (ΔS_a) from the slop and intercept plot of ln (i_{corr}/T) vs. $1/T$ [67]:

$$i_{\text{corr}} = \frac{RT}{NH}\exp\left(\frac{\Delta Sa}{R}\right)\exp\left(\frac{\Delta Ha}{RT}\right) \tag{9}$$

where N is Avogadro's number and h is Plank's constant.

In the absence and presence of CH-ZnONPs at various temperatures, along with Arrhenius and transition state plots, the potentiodynamic polarisation curves for mild steel corrosion are shown in Figure 5.

Results showed that with temperature increase, inhibition efficiencies of CH-ZnONPs for mild steel corrosion in the acid medium decreased. This decrease in the inhibition efficiency of CH-ZnONPs may be due to adsorbed inhibitor desorption. In addition, it can be shown that in the presence of CH-ZnONPs, the values of activation energies (69.43 KJ mol^{-1}) are much higher than in their absence (35.38 KJ mol^{-1}) [68]. This finding further indicates that in the presence of CH-ZnONPs composite molecules, mild steel corrosion becomes difficult due to their adsorption on the metal surface and the formation of inhibitive films. Higher and positive values of ΔH_a suggest that the endothermic phase is the corrosion of mild steel with (66.9 KJ mol^{-1}) and without inhibitor (32.8 KJ mol^{-1}) (CH-ZnONPs) molecules [68]. Relatively lower ΔH_a values than E_a values ($E_a > \Delta H_a$) suggest that the findings obtained in the current study are compatible with the thermodynamic relationship ($E_a - \Delta H_a = RT$) [68]. It can also be shown that in the presence of inhibitors (CH-ZnONPs nanocomposite), the values of ΔS_a (−12.61 KJ mol^{-1}) are more favourable than that of their absence (−81. 21KJ mol^{-1}) due to the displacement by the inhibitor (CH-ZnONPs composite) molecules of pre-adsorbed water molecules.

3.5 Surface morphology analysis

SEM is an important part of the analysis of surface corroded and uncorroded metal in the morphological use of the surface mild steel. Adequacy of the surface morphology of mild steel without and with 100 ppm CH-ZnO is measured for the corrosion inhibiting properties of chitosan

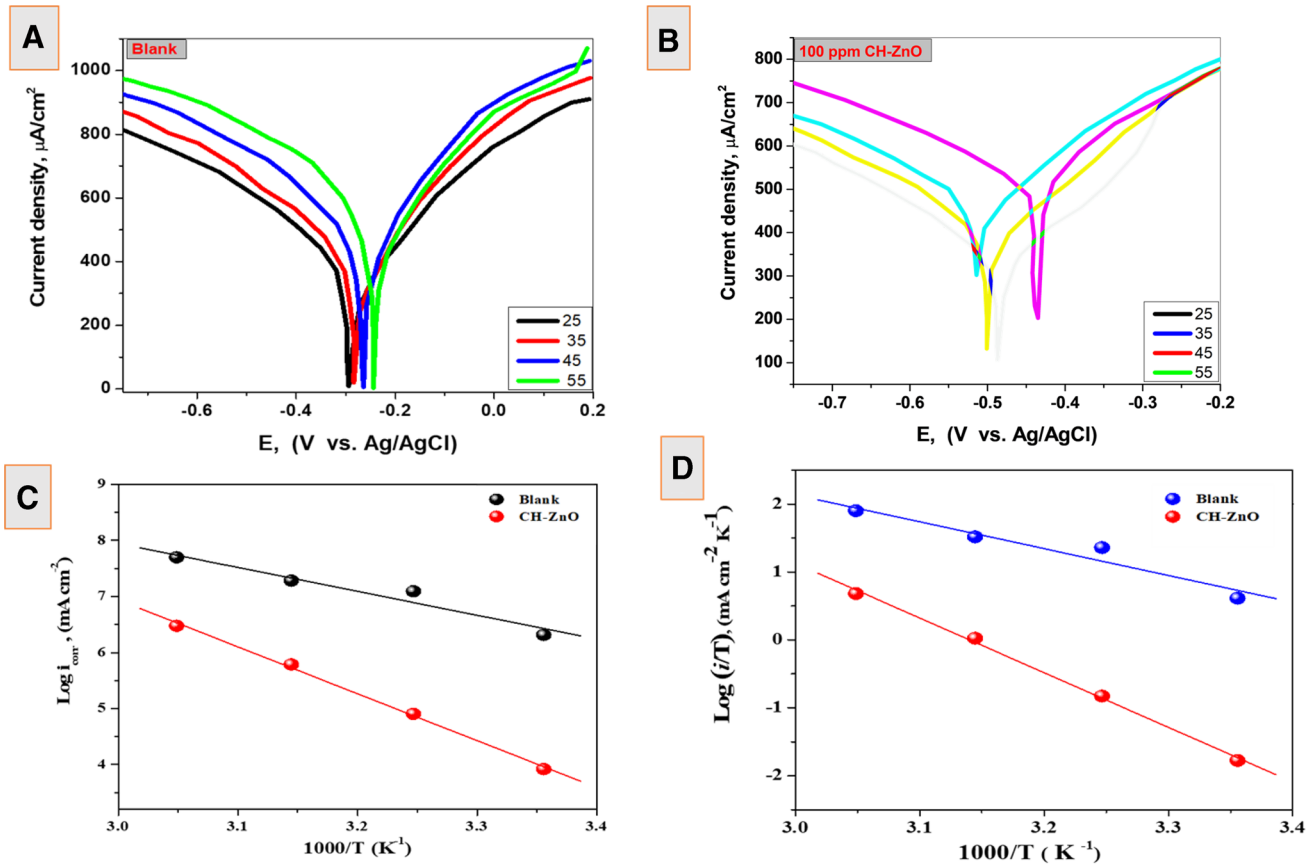

Figure 5 Potentiodynamic polarisation curves of mild steel in 1 M HCl solution at different temperatures **B** 100 ppm CH-ZnONPs nanoparticles at different temperatures. **C** Activation and **D** transition state for mild steel corrosion in 1 M HCl with and without *CH-ZnONPs* nanoparticles.

composite. After 24 h of immersion in that certain solution, the electron scanning microscopy images were taken (Figure 6). The first image (Figure 6A) shows an inhibitor-free damaged surface. In particular, a clear inhomogeneous surface with great cracks showed unprotected mild steel. However, the sample surface is much clean and smooth in second image (Figure 6B). EDS analysis detects Fe-, O-, C-, N- and Zn-containing compounds. The results of the EDS test are valuable evidence to support the decreased Fe content and increase of the oxygen and carbon content, which confirm the adsorption of compounds in CH-ZnONPS on the surface of mild steel in addition to presence of N and Zn from inhibitor molecules.

Measurement of roughness is a valid test to provide data about the ability of an electrode surface to avoid severe damage and the generation of passive layers. AFM topographic images were shown in order to investigate the morphological characteristics of the surface quantitatively (Figure 6E–F). The addition of 100 ppm of CH-ZnONPs has shown a decreased mean roughness (S_a) of the specimen (i.e., for blank samples $S = 113$ nm and $S_a = 42$ nm for the inhibited specimen). This could greatly hinder the corrosion of the steel surface due to the adsorption of CH-ZnONP molecules, resulting in cleaner surface area with lower wells and damaged areas.

3.6 Antimicrobial study

Antimicrobial activity was evaluated via CFU methods according to the tested sample solubility. The popular microorganisms include gram positive, gram negative, filamentous fungi and unicellular fungi. Neat chitosan was offered moderate antimicrobial activity against all tested organisms. The antimicrobial activity was enhanced with more than 3-fold in the case of CH-ZnONPs (Fig. 7). These results may be due to the synergistic effect of Ch and ZnO nanoparticles where the chitosan mechanism of action focusing on positive charge which located in amino group which denaturation the out layer of microbial cell [33, 69]. Additionally, ZnO nanoparticle mechanism of action summarised as disruption of the cell membrane and oxidative stress [70, 71].

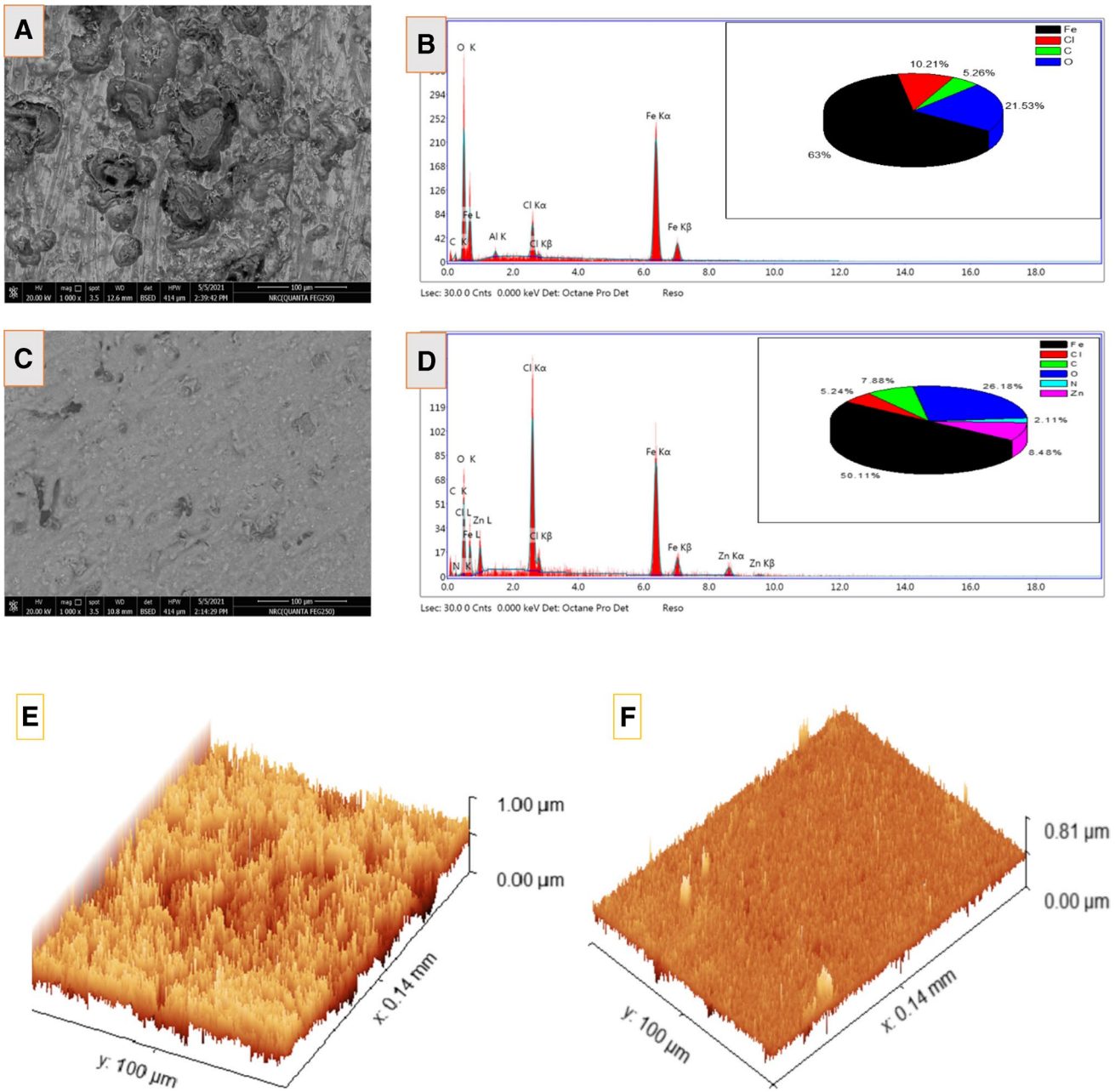

Figure 6. SEM image and EDX of mild steel after immersion for 24 h in 1 M HCl without (**A**, **B**) and with 100 ppm CH-ZnO (**C**, **D**), roughness measurement of mild steel after immersion for 24 h in 1 M HCl without (**E**) and with 100 ppm CH-ZnO (F).

4 Conclusion

Chitosan-zinc oxide composite was synthesised, characterised and tested using electrochemical, surface morphology as inhibitors of mild steel corrosion in 1 M HCl. The study of electrochemical impedance spectroscopy (EIS) found that CH-ZnONPs composite molecules acted as corrosion inhibitors of the interface form. The potentiodynamic polarisation study suggests that CH-ZnONPs composite acted as mixed-type inhibitors and they affect the rate of anodic and cathodic Tafel polarisation reactions. Potentiodynamic polarisation studies also indicate that by blocking the active sites on the steel through adsorption on the metallic surface, CH-ZnONPs composite inhibit corrosion of mild steel in the aggressive acid solution. The Langmuir adsorption isotherm was obtained by adsorption of CH-ZnONPs composite molecules on the steel surface. In addition, the antimicrobial activity study has clarified the attention of the prepared nanocomposite as broad-spectrum antimicrobial agent.

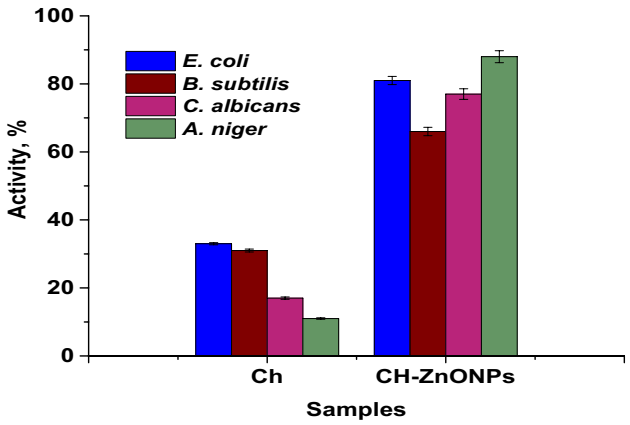

Figure 7. Antimicrobial activity of neat chitosan and CH-ZnONPs.

Funding This study is funded by the National Research Centre (NRC), Egypt.

Declarations

Competing interests The authors declare no competing interests.

References

1. F Bentiss M Traisnel M Lagrenee 2000 The substituted 1, 3, 4-oxadiazoles: a new class of corrosion inhibitors of mild steel in acidic media. Corros Sci 42(1):127–146
2. M Rbaa 2018 Synthesis, characterization and corrosion inhibition studies of novel 8-hydroxyquinoline derivatives on the acidic corrosion of mild steel: Experimental and computational studies Materials discovery 12 43 54
3. S Abd El-Rehim MA Ibrahim K Khaled 1999 4-Aminoantipyrine as an inhibitor of mild steel corrosion in HCl solution Journal of Applied Electrochemistry 29 5 593 599
4. S Abd El Rehim MA Ibrahim K Khalid 2001 The inhibition of 4-(2′-amino-5′-methylphenylazo) antipyrine on corrosion of mild steel in HCl solution Materials Chemistry and Physics 70 3 268 273
5. M Kermani D Harrop 1996 The impact of corrosion on oil and gas industry SPE Prod Facil 11 03 186 190
6. J Haque 2021 Corrosion inhibition of mild steel in 1M HCl using environmentally benign Thevetia peruviana flower extracts Sustainable Chemistry and Pharmacy 19 100354
7. F El-Hajjaji 2020 Electrochemical and theoretical insights on the adsorption and corrosion inhibition of novel pyridinium-derived ionic liquids for mild steel in 1 M HCl Journal of Molecular Liquids 314 113737
8. A Rahimi 2021 Development of a novel thermally stable inhibitor based on furfuryl alcohol for mild steel corrosion in a 15% HCl medium for acidizing application Ind Eng Chem Res 60 30 11030 11044
9. M Zhang 2021 Akebia trifoliate koiaz peels extract as environmentally benign corrosion inhibitor for mild steel in HCl solutions: integrated experimental and theoretical investigations J Ind Eng Chem 101 227 236
10. AR Shahmoradi 2021 Theoretical and surface/electrochemical investigations of walnut fruit green husk extract as effective inhibitor for mild-steel corrosion in 1M HCl electrolyte Journal of Molecular Liquids 338 116550
11. MM Solomon 2018 Exploration of dextran for application as corrosion inhibitor for steel in strong acid environment: effect of molecular weight, modification, and temperature on efficiency ACS Appl Mater Interfaces 10 33 28112 28129
12. D Jayaperumal 2010 Effects of alcohol-based inhibitors on corrosion of mild steel in hydrochloric acid Mater Chem Phys 119 3 478 484
13. E Oguzie 2010 Adsorption and corrosion-inhibiting effect of Dacryodis edulis extract on low-carbon-steel corrosion in acidic media J Colloid Interface Sci 349 1 283 292
14. M Prabakaran 2017 Aster koraiensis as nontoxic corrosion inhibitor for mild steel in sulfuric acid J Ind Eng Chem 52 235 242
15. LL Liao 2018 Corrosion protection for mild steel by extract from the waste of lychee fruit in HCl solution: Experimental and theoretical studies J Colloid Interface Sci 520 41 49
16. A Moradi 2021 Molecular dynamic (MD) simulation and electrochemical assessments of the Satureja Hortensis extract for the construction of effective zinc-based protective film on carbon steel Journal of Molecular Liquids 338 116606
17. P Okafor 2008 Inhibitory action of Phyllanthus amarus extracts on the corrosion of mild steel in acidic media Corros Sci 50 8 2310 2317
18. A El-Sayed 1997 Phenothiazine as inhibitor of the corrosion of cadmium in acidic solutions J Appl Electrochem 27 2 193 200
19. GK Gomma MH Wahdan 1994 Temperature coefficient of corrosion inhibition of steel by adenine Bull Chem Soc Jpn 67 10 2621 2626
20. K Zhang 2018 Inhibitory effect of konjac glucomanan on pitting corrosion of AA5052 aluminium alloy in NaCl solution J Colloid Interface Sci 517 52 60
21. MS Hasanin SA Al Kiey 2020 Environmentally benign corrosion inhibitors based on cellulose niacin nano-composite for corrosion of copper in sodium chloride solutions. International Journal of Biological Macromolecules 161:345–354
22. E Abd El Meguid S Abd El Rehim S Al Kiey 2016 Inhibitory effect of cetyltrimethyl ammonium bromide on the corrosion of 904L stainless steel in LiBr solution Corrosion Engineering, Science and Technology 51 6 429 437
23. L Jiang 2018 Excellent corrosion inhibition performance of novel quinoline derivatives on mild steel in HCl media: experimental and computational investigations J Mol Liq 255 53 63
24. Y Sasikumar 2015 Experimental, quantum chemical and Monte Carlo simulation studies on the corrosion inhibition of some alkyl imidazolium ionic liquids containing tetrafluoroborate anion on mild steel in acidic medium J Mol Liq 211 105 118
25. M Talari 2019 Experimental and computational chemistry studies of two imidazole-based compounds as corrosion inhibitors for mild steel in HCl solution Journal of Molecular Liquids 286 110915
26. SA Umoren UM Eduok 2016 Application of carbohydrate polymers as corrosion inhibitors for metal substrates in different media: a review Carbohyd Polym 140 314 341
27. K Zhang 2018 Amino acids modified konjac glucomannan as green corrosion inhibitors for mild steel in HCl solution Carbohyd Polym 181 191 199
28. Q Zhao 2020 Chitosan derivatives as green corrosion inhibitors for P110 steel in a carbon dioxide environment Colloids and Surfaces B: Biointerfaces 194 111150
29. Shahini M, B Ramezanzadeh, and HE Mohammadloo 2020 Recent advances in biopolymers/carbohydrate polymers as

effective corrosion inhibitive macro-molecules: a review study from experimental and theoretical views. J Mol Med 115110
30. Al Kiey, Sherief A, Hasanin, Mohamed S, Dacrory, Sawsan, 2021 Potential anticorrosive performance of green and sustainable inhibitor based on cellulose derivatives for carbon steel. J Mol Med 338:116604
31. Shehabeldine A, Hasanin M, Monitoring, and Management 2019 Green synthesis of hydrolyzed starch–chitosan nano-composite as drug delivery system to gram negative bacteria. 12:100252
32. Hasanin M, Labeeb AM Dielectric properties of nicotinic acid/methyl cellulose composite via "green" method for anti-static charge applications. Mater Sci Eng B 263:114797
33. Salama A, Hasanin M, Hesemann P 2020 Synthesis and antimicrobial properties of new chitosan derivatives containing guanidinium groups. 241:116363
34. J Varshosaz S Eskandari M Tabbakhian 2012 Freeze-drying of nanostructure lipid carriers by different carbohydrate polymers used as cryoprotectants Carbohyd Polym 88 4 1157 1163
35. H Tang 2005 Important role of starch in the freeze-thaw damage of Nama-An particles prepared from adzuki beans (Vigna angularis) Carbohyd Polym 59 2 197 204
36. Mehrez E El-Naggar, Mohamed Hasanin, Ahmed M Youssef, Ali Aldalbahi, Mohamed H El-Newehy, Reda M Abdelhameed 2020 Hydroxyethyl cellulose/bacterial cellulose cryogel dopped silver@ titanium oxide nanoparticles: Antimicrobial activity and controlled release of Tebuconazole fungicide 165:1010–1021
37. Turky G, Moussa MA, Hasanin M, El-Sayed NS, Kamel S 2020 Carboxymethyl cellulose-based hydrogel: dielectric study, antimicrobial activity and biocompatibility. 1–14
38. A Youssef 2021 Conducting chitosan/hydroxylethyl cellulose/polyaniline bionanocomposites hydrogel based on graphene oxide doped with Ag-NPs. 167 1435 1444
39. K Rasool DS Lee 2016 Effect of ZnO nanoparticles on biodegradation and biotransformation of co-substrate and sulphonated azo dye in anaerobic biological sulfate reduction processes Int Biodeterior Biodegradation 109 150 156
40. X Yan 2015 Effects of ZnO nanoparticles on dimethoate-induced toxicity in mice J Agric Food Chem 63 37 8292 8298
41. ML Zheludkevich 2011 Self-healing protective coatings with "green" chitosan based pre-layer reservoir of corrosion inhibitor J Mater Chem 21 13 4805 4812
42. M Abdelraof 2019 Green synthesis of bacterial cellulose/bioactive glass nanocomposites: Effect of glass nanoparticles on cellulose yield Biocompatibility and antimicrobial activity. 138 975 985
43. M Abdelraof 2020 Immobilization of L-methionine γ-lyase on different cellulosic materials and its potential application in green-selective synthesis of volatile sulfur compounds. 8 4 103870
44. YA Selim 2020 Green synthesis of zinc oxide nanoparticles using aqueous extract of deverra tortuosa and their cytotoxic activities Sci Rep 10 1 3445
45. Ibrahim S, El Saied H, Hasanin M 2019 Active paper packaging material based on antimicrobial conjugated nano-polymer/amino acid as edible coating. 31(4): 1095–102
46. C Verma EE Ebenso M Quraishi 2017 Ionic liquids as green and sustainable corrosion inhibitors for metals and alloys: an overview J Mol Liq 233 403 414
47. LL Liao 2017 Longan seed and peel as environmentally friendly corrosion inhibitor for mild steel in acid solution: experimental and theoretical studies J Colloid Interface Sci 499 110 119
48. B Hirschorn 2010 Determination of effective capacitance and film thickness from constant-phase-element parameters Electrochim Acta 55 21 6218 6227
49. M Zheludkevich 2007 On the application of electrochemical impedance spectroscopy to study the self-healing properties of protective coatings Electrochem Commun 9 10 2622 2628
50. B Fernández-Pérez 2014 Electrochemical impedance spectroscopy investigation of the corrosion resistance of a waterborne acrylic coating containing active electrochemical pigments for the protection of carbon steel Int J Electrochem Sci 9 4 2067
51. I Ahamad R Prasad M Quraishi 2010 Thermodynamic, electrochemical and quantum chemical investigation of some Schiff bases as corrosion inhibitors for mild steel in hydrochloric acid solutions Corros Sci 52 3 933 942
52. E Westing Van G Ferrari J Wit De 1993 The determination of coating performance with impedance measurements-I Coating polymer properties. Corrosion Science 34 9 1511 1530
53. C Verma 2018 Melamine derivatives as effective corrosion inhibitors for mild steel in acidic solution: chemical, electrochemical, surface and DFT studies Results in Physics 9 100 112
54. D Ribeiro C Souza J Abrantes 2015 Use of Electrochemical Impedance Spectroscopy (EIS) to monitoring the corrosion of reinforced concrete Revista IBRACON de Estruturas e Materiais 8 4 529 546
55. S Cao 2019 Corrosion inhibition effects of a novel ionic liquid with and without potassium iodide for carbon steel in 0.5 M HCl solution: an experimental study and theoretical calculation Journal of Molecular Liquids 275 729 740
56. P Han 2018 Synergistic effect of mixing cationic and nonionic surfactants on corrosion inhibition of mild steel in HCl: experimental and theoretical investigations J Colloid Interface Sci 516 398 406
57. M Rbaa 2019 Two new 8-hydroxyquinoline derivatives as an efficient corrosion inhibitors for mild steel in hydrochloric acid: synthesis, electrochemical, surface morphological, UV–visible and theoretical studies J Mol Liq 276 120 133
58. A Chaouiki 2018 Understanding corrosion inhibition of mild steel in acid medium by new benzonitriles: Insights from experimental and computational studies J Mol Liq 266 603 616
59. TNJI Edison 2018 Corrosion inhibition performance of spermidine on mild steel in acid media J Mol Liq 264 483 489
60. M Yadav 2016 Corrosion inhibition performance of pyranopyrazole derivatives for mild steel in HCl solution: Gravimetric, electrochemical and DFT studies J Mol Liq 216 78 86
61. M Yadav 2015 Synthesis and application of new acetohydrazide derivatives as a corrosion inhibition of mild steel in acidic medium: insight from electrochemical and theoretical studies Journal of molecular liquids 208 322 332
62. I Obot N Obi-Egbedi 2010 Indeno-1-one [2, 3-b] quinoxaline as an effective inhibitor for the corrosion of mild steel in 0.5 M H2SO4 solution Materials Chemistry and Physics 122 2–3 325 328
63. MM Solomon H Gerengi SA Umoren 2017 Carboxymethyl cellulose/silver nanoparticles composite: synthesis, characterization and application as a benign corrosion inhibitor for St37 steel in 15% H2SO4 medium ACS Appl Mater Interfaces 9 7 6376 6389
64. H Lgaz 2017 Effect of clozapine on inhibition of mild steel corrosion in 1.0M HCl medium Journal of Molecular Liquids 225 271 280
65. M Srivastava 2017 Electrochemical investigation of Irbesartan drug molecules as an inhibitor of mild steel corrosion in 1M HCl and 0.5M H2SO4 solutions Journal of Molecular Liquids 236 184 197
66. A Mishra 2018 Synthesis, characterization and corrosion inhibition studies of N-phenyl-benzamides on the acidic corrosion of mild steel: experimental and computational studies J Mol Liq 251 317 332
67. S Shahabi 2019 Synthesis, experimental, quantum chemical and molecular dynamics study of carbon steel corrosion inhibition effect of two Schiff bases in HCl solution J Mol Liq 285 626 639

68. A Zarrouk 2013 Theoretical approach to the corrosion inhibition efficiency of some quinoxaline derivatives of steel in acid media using the DFT method Res Chem Intermed 39 3 1125 1133
69. M Kong 2010 Antimicrobial properties of chitosan and mode of action: a state of the art review Int J Food Microbiol 144 1 51 63
70. Y Xie 2011 Antibacterial activity and mechanism of action of zinc oxide nanoparticles against Campylobacter jejuni Applied and Environmental Microbiology 77 7 2325
71. D Sardella R Gatt VP Valdramidis 2017 Physiological effects and mode of action of ZnO nanoparticles against postharvest fungal contaminants Food Res Int 101 274 279